Atmospheric
Chemistry
and Physics

Open Access

EGU

Discussions

1 **Value-added by high-resolution regional simulations of**

2 **climate-relevant aerosol properties**

3

4 P. Crippa[1], R. C. Sullivan[2], A. Thota[3], S. C. Pryor[2,3]

5

6

7 [1]COMET, School of Civil Engineering and Geosciences, Cassie Building, Newcastle

8 University, Newcastle upon Tyne, NE1 7RU, UK

9 [2]Department of Earth and Atmospheric Sciences, Bradfield Hall, 306 Tower Road, Cornell

10 University, Ithaca, NY 14853, USA

11 [3]Pervasive Technology Institute, Indiana University, Bloomington, IN 47405, USA

12

13 *Correspondence to:* P. Crippa (paola.crippa@ncl.ac.uk), School of Civil Engineering and

14 Geosciences, Cassie Building, Room G15, Telephone: +44 (0)191 208 5041, Newcastle

15 University, Newcastle upon Tyne, NE1 7RU, UK

Atmospheric
Chemistry
and Physics
Discussions

Open Access

EGU

16 **Abstract**

17 Despite recent advances in global Earth System Models (ESMs), the current global mean

18 aerosol direct and indirect radiative effects remain uncertain, as does their future role in climate

19 forcing and regional manifestations. Reasons for this uncertainty include the high spatio-

20 temporal variability of aerosol populations. Thus, limited area (regional) models applied at

21 higher resolution over specific regions of interest are generally expected to 'add value', i.e.

22 improve the fidelity of the physical-dynamical-chemical processes that induce extreme events

23 and dictate climate forcing, via more realistic representation of spatio-temporal variability.

24 However, added value is not inevitable, and there remains a need to optimize use of numerical

25 resources, and to quantify the impact on simulation fidelity that derives from increased

26 resolution. Here we quantify the value added by enhanced spatial resolution in simulations of

27 the drivers of aerosol direct radiative forcing by applying the Weather Research and

28 Forecasting model with coupled Chemistry (WRF-Chem) over eastern North America at

29 different resolutions. Using Brier Skill Scores and other statistical metrics it is shown that

30 enhanced resolution (from 60 to 12 km) improves model performance for all of the

31 meteorological parameters and gas phase concentrations considered, in addition to both mean

32 and extreme Aerosol Optical Depth (AOD) in three wavelengths in the visible relative to

33 satellite observations, principally via increase of potential skill. Some of the enhanced model

34 performance for AOD appears to be attributable to improved simulation of specific humidity

35 and the resulting impact on aerosol hygroscopic growth/hysteresis.

36

37 **Keywords:** added value, high-resolution WRF-Chem simulations, aerosol optical properties,

38 extreme AOD

Atmospheric
Chemistry
and Physics
Discussions

1 Motivation and Objectives

Aerosols alter Earth's radiation balance primarily by scattering or absorbing incoming solar radiation (direct effect, dominated by accumulation mode (diameters ~ wavelength (λ), where total extinction is often quantified using AOD), or regulating cloud formation/properties by acting as cloud condensation nuclei (CCN) (indirect effect, dominated by diameters $\geq$ 100 nm, magnitude = f(composition)). Most aerosols (excluding black carbon) have a larger scattering cross-section than absorption cross-section, and act as CCN thus enhancing cloud albedo and lifetimes. Hence increased aerosol concentrations are generally (but not uniformly) associated with surface cooling (offsetting a fraction of greenhouse gas warming) (Boucher, 2013;Myhre et al., 2013b) to a degree that is principally dictated by the aerosol concentration, size and composition, in addition to the underlying surface and height of the aerosol layer (McComiskey et al., 2008). Despite major advances in measurement and modeling, both the current global mean aerosol direct effect (possible range: -0.77 to +0.23 W m^{-2}) and the indirect effect (possible range: -1.33 to -0.06 W m^{-2}) remain uncertain, as does their future role in climate forcing (Rockel et al., 2008) and regional manifestations (Myhre et al., 2013a). Specific to our current study region (eastern N. America), one analysis using the NASA GISS global model found that the "regional radiative forcing from US anthropogenic aerosols elicits a strong regional climate response, cooling the central and eastern US by 0.5–1.0 °C on average during 1970–1990, with the strongest effects on maximum daytime temperatures in summer and autumn. Aerosol cooling reflects comparable contributions from direct and indirect radiative effects" (Leibensperger et al., 2012). A recent comparison of multiple global models conducted under the AEROCOM-project indicated this is also a region that exhibits very large model-to-model variability in simulated AOD (<AOD> ~ 0.5, σ(AOD) ~ 1) (Myhre et al., 2013a).

Major reasons why aerosol radiative forcing on both the global and regional scales remains uncertain include short atmospheric residence times and high spatio-temporal variability of aerosol populations, and the complexity of the processes that dictate aerosol concentrations, composition and size distributions (Seinfeld and Pandis, 2016). Although aerosol processes and properties are increasingly being treated in the global Earth System Models (ESMs) (Long et al., 2015;Tilmes et al., 2015) being applied in Coupled Model Intercomparison Project Phase 6 (CMIP-6) (Meehl et al., 2014), the scales on which such models are applied remain much coarser than those on which aerosol population properties are known to vary (Anderson et al., 2003). Therefore, limited area atmospheric models (regional models) applied at higher resolution over specific regions of interest are expected to 'add value' (i.e. improve the fidelity)

Atmospheric
Chemistry
and Physics
Discussions

72   of the physical-dynamical-chemical processes that induce extreme events and dictate climate

73   forcing. However, debate remains regarding how to objectively evaluate model performance,

74   quantify the value added by enhanced resolution (Di Luca et al., 2015;Rockel et al., 2008) and

75   on possible limits to the improvement of climate representation in light of errors in the driving

76   "imperfect lateral boundary conditions" (Diaconescu and Laprise, 2013). Nevertheless,

77   although "it is unrealistic to expect a vast amount of added values since models already

78   performs rather decently" (Di Luca et al., 2015) and global ESMs are now run at much higher

79   resolution than in the past, it is generally assumed that high resolution regional models will add

80   value via more realistic representation of spatio-temporal variability than global coarser-

81   resolution simulations.

82   Here we quantify the value added by enhanced resolution in the description of the drivers of

83   aerosol direct radiative forcing using simulations from WRF-Chem over eastern North

84   America. The primary performance evaluation focuses on AOD at the different wavelengths

85   (λ = 470, 550 and 660 nm, where the AOD at different λ is used as a proxy of the aerosol size

86   distribution (Tomasi et al., 1983), see details in Sect. 2.1) and is measured relative to

87   observations from satellite-borne instrumentation. Thus the term "value added" is used here to

88   refer to an improvement of model performance in simulation of wavelength specific AOD as

89   measured by the MODerate resolution Imaging Spectroradiometer (MODIS) instrument

90   aboard the polar-orbiting Terra satellite. We begin by quantifying the performance of WRF-

91   Chem when applied over eastern North America at a resolution of 60 km (WRF60) (~ finest

92   resolution likely to be employed in CMIP-6 global simulations) and then compare the results

93   to those from simulations conducted at 12 km (WRF12) (simulation details are given in Table

94   S1). Quantification of model skill is undertaken by mapping the WRF12 output to the WRF60

95   grid (WRF12-remap) and computing Brier Skill Scores (BSS) using MODIS as the target,

96   WRF60 as the reference forecast and WRF12-remap as the forecast to be evaluated. We also

97   evaluate the impact of simulation resolution on extreme AOD values that are associated with

98   enhanced impacts on climate and human health. This analysis uses both *Accuracy* and *Hit Rate*

99   as the performance metrics and focuses on the co-occurrence of extreme values in space from

100   the model output and MODIS.

101   Our final analysis focuses on evaluation of the value-added by enhanced resolution in terms of

102   key meteorological and gas-phase drivers of aerosol concentrations and composition and is

103   conducted relative to the MERRA-2 reanalysis product for the physical variables and columnar

104   gas concentrations from satellite observations (see details of the precise data sets used given

Atmospheric
Chemistry
and Physics
Discussions

Open Access

EGU

105   below). The meteorological parameters considered are air temperature at 2 m (T_{2m}), total

106   monthly precipitation (*PPT*), planetary boundary-layer height (*PBLH*) and specific humidity

107   in the boundary layer (Q_{PBL}). The gas phase concentrations considered are: sulfur dioxide

108   (SO_2), ammonia (NH_3), nitrogen dioxide (NO_2) and formaldehyde (HCHO).

2 Materials and Methods

2.1 Spectral dependence of AOD

111   Three properties dictate the actual aerosol direct radiative forcing: AOD, single scattering

112   albedo and asymmetry factor, all of which are a function of the wavelength (λ) of incident

113   radiation. The first property is related to the total columnar mass loading, typically dominates

114   the variability of direct aerosol effect (Chin et al., 2009) and is the focus of the current research.

115   The relationship between the aerosol size distribution and spectral dependence of AOD is

116   discussed in detail in (Tomasi et al., 1983) but can be understood by considering a simplified

117   example:

118    $$\beta(\lambda) = \beta(\lambda = 1\mu m) \times \lambda^{-\alpha} \quad (1)$$

119   where β is the particle extinction coefficient, λ is the wavelength and α is the Ångström

120   exponent (Ångström, 1964) which describes the wavelength dependence of AOD (and is

121   inversely proportional to the average aerosol Dp):

122    $$\alpha = \frac{\ln \frac{AOD(\lambda_1)}{AOD(\lambda_2)}}{\frac{\lambda_2}{\lambda_1}} \quad (2)$$

123   Using Mie theory for spherical particles with radius (*r*): 0.1-1 µm, if the aerosol size

124   distribution is described by the Junge power law (Eq. 3) then α ~ ν-2 (i.e. α~1):

125    $$\frac{dN}{d\ln(r)} = K \times r^{-\nu} \quad (3)$$

126   where *dN* is the number of particles of size falling within the radius interval dln(*r*), *K* is a

127   constant (function of particle total number concentration) and *ν* is the Junge parameter (*ν* is

128   typically of the order of 2-3 for *r* < 10 µm and decreases with increasing proportion of coarse

129   aerosols) (Tomasi et al., 1983). Thus, aerosol populations with a higher proportion of coarse

130   mode aerosols will, on average, exhibit higher AOD in the longer wavelengths.

Atmospheric
Chemistry
and Physics
Discussions

2.2 WRF-Chem simulations

WRF-Chem (version 3.6.1) simulations were performed for the year 2008 over eastern North America, in a domain centered over southern Indiana (86°W, 39°N) at two resolutions, one close to the finest resolution designed for CMIP-6 global model runs (i.e. 60 km, WRF60) and the other one at much higher resolution (12 km, WRF12). Simulation settings are identical for the two runs except for the time-step used for the physics (Table S1), and include use of a modal representation of the aerosol size distribution with three lognormal modes and fixed geometric standard deviations ($\sigma_{g,Aitken}$=1.6 and $\sigma_{g,accumulation}$=2, (Ackermann et al., 1998;Grell et al., 2005)) and telescoping vertical grid with 10 model layers from the surface to 800 hPa. Meteorological initial and boundary conditions from the North American Mesoscale Model at 12 km resolution are applied every 6 hours, while initial and chemical boundary conditions are taken from MOZART-4 (Model for Ozone and Related chemical Tracers, version 4) with meteorology from NCEP/NCAR-reanalysis (Emmons et al., 2010). Anthropogenic emissions are specified for both WRF60 and WRF12 from the US National Emission Inventory 2005 (NEI-05) (US-EPA, 2009) which provides hourly point and area emissions at 4 km on 19 vertical levels. The simulation settings and specifically the use of a modal representation of the aerosol size distribution were selected to retain computational tractability. Accordingly, the 60 km simulations for the year 2008 completed in 6.4 hours whereas the 12 km simulations completed in 9.5 days (230 hours) on the Cray XE6/XK7 supercomputer (Big Red II) owned by Indiana University, using 256 processors distributed on 8 nodes.

Value added is quantified by degrading (averaging) hourly output from the 12 km resolution simulation to 60 km (hereafter WRF12-remap) as follows: the 12 km domain is resized excluding 2 grid cells at the border to exactly match the 60 km resolution domain. Each coarse grid cell thus includes 5×5 12 km resolution cells and its value is the mean of all valid 12 km grid cells inside it if at least half of those cells contain valid AOD (i.e. no cloud cover), otherwise the whole coarse cell is treated as missing. In all comparisons only cells with simultaneous (i.e. model and MODIS) clear sky conditions are considered. A daily value is computed for the satellite overpass time, while a monthly mean is computed using values during the overpass hour and under clear sky conditions if there are at least five valid observations in the month.

2.3 Observations

Model aerosol optical properties are evaluated relative to the MODIS Collection 6 dark-target

Atmospheric
Chemistry
and Physics
Discussions

Open Access

EGU

163   land aerosol product from aboard the Terra satellite (~1030 overpass local solar time (LST))

164   (Levy et al., 2013). Trace gas concentrations are evaluated relative to measurements from the

165   Ozone Monitoring Instrument (OMI; version 3) (Chance, 2002) and the Infrared Atmospheric

166   Sounding Interferometer (IASI; NN version 1) (Whitburn, 2016) aboard the Aura (~1345 LST)

167   and MetOp satellites (~0930 LST), respectively. MODIS retrieves AOD at multiple λ including

168   470, 550, and 660 nm. The MODIS algorithm removes cloud-contaminated pixels prior to

169   spatial averaging over 10×10 km (at nadir). OMI and IASI have nadir resolutions of 13×24

170   km and 12 km (circular footprint), respectively, and have been filtered to remove retrievals

171   with cloud fractions > 0.3 (Fioletov et al., 2011;McLinden et al., 2014;Vinken et al., 2014) and

172   OMI pixels affected by the row anomalies. Uncertainty in AOD from MODIS is spatially and

173   temporally variable. It has been estimated as $\pm 0.05 \pm 0.15 \times$ AOD over land (Levy et al., 2013),

174   and prior research has reported 71% of MODIS Collection 5 retrievals fall within $\pm 0.05 \pm 0.2$

175    $\times$ AOD relative to AERONET in the study domain (Hyer et al., 2011). The accuracy of OMI

176   ("root sum of the square of all errors, including forward model, inverse model, and instrument

177   errors" (Brinksma, 2003)) is 1.1 DU or 50% for SO_2, 2×10^{14} cm^{-2}/30% for

178   background/polluted NO_2 conditions, and 35% for HCHO. This uncertainty is typically

179   reduced by spatial and temporal averaging, as described below (Fioletov et al., 2011;Krotkov

180   et al., 2008). IASI NH_3 retrievals do not use an a priori assumption of emissions, vertical

181   distribution, or lifetime of NH_3 (i.e. no averaging kernel); therefore, NH_3 accuracy is variable,

182   and thus only retrievals with uncertainty lower than the retrieved concentrations are used

183   (Whitburn, 2016).

184   For the model evaluation, MODIS AOD; OMI SO_2, NO_2, and HCHO; and IASI NH_3 for each

185   day are regridded to the WRF-Chem domain by averaging all valid retrievals within 0.1° and

186   0.35°; 0.125° × 0.18° and 0.365° × 0.42°; and 0.12° and 0.36° of each WRF-Chem grid cell

187   centroid, for the 12×12 km and 60×60 km resolutions, respectively. To avoid issues from

188   under-sampling, we require at least 10 valid MODIS granules for the 60×60 km daily average

189   to be computed and at least 5 daily averages to compute a monthly average for each grid cell.

190   Model evaluation of gaseous species is performed on standard scores (z-scores) computed

191   relative to the spatial mean of each month, which allow comparing spatial patterns of satellite

192   observations and model output in terms of standard deviation units from the mean.

193   The simulated meteorological properties are evaluated using Modern-Era Retrospective

194   analysis for Research and Applications (MERRA-2) reanalysis data as the target. MERRA-2

Atmospheric
Chemistry
and Physics
Discussions

195   is a homogenized and continuous in time description of atmospheric properties on a 3-

196   dimensional global grid (horizontal resolution of 0.5°×0.625°, L72), developed by NASA and

197   was released in Fall 2015 (Molod et al., 2015). MERRA-2 provides hourly values of T_{2m} and

198   *PBLH*, and vertical profile of 3-dimensional variables every 3 hours on a large number of

199   pressure levels. Here we compute the total specific humidity (Q_{PBL}) of the lowest 8 pressure

200   levels (i.e. in the boundary-layer approximated as the layer from 1000 to 825 hPa) in MERRA-

201   2, assuming an average air density in the PBL of 1.1 kg m^{-3}. For the evaluation of simulated

202   precipitation, we use accumulated monthly total values.

203   **2.4 Quantification of model performance and added-value**

204   Taylor diagrams summarize three aspects of model performance relative to a reference: the

205   spatial correlation coefficient (i.e. Pearson correlation of the fields, r), the ratio of spatial

206   standard deviations of the two spatial fields ($\sigma_{wrf}/\sigma_{sat}$) and the root mean squared difference

207   (Taylor, 2001). Here Taylor diagrams are presented for monthly mean AOD from WRF60,

208   WRF12 and WRF12-remap relative to MODIS at different wavelengths (Fig. 1). Because AOD

209   is not normally distributed, Spearman's rank correlation coefficients (ρ) of the mean monthly

210   AOD spatial fields are also computed to reduce the impact of a few outliers and the small

211   sample size during cold months (Table 1). To assess the significance of ρ while accounting for

212   multiple testing, we apply a Bonferroni correction (Simes, 1986) in which for *m* independent

213   hypothesis tests, the null hypothesis is rejected if $p \leq \dfrac{\alpha}{m}$, where *p* is the p-value and α is the

214   confidence level (0.05 is used here).

215   We further quantify the value added (or lack of thereof) of the high-resolution simulations

216   using the following metrics:

217   **(i) Brier Skill Score**

218   The primary metric used to quantify the added value of WRF12-remap versus WRF60 is the

219   Brier Skill Score (BSS) (Murphy and Epstein, 1989):

220
$$BSS = \frac{r_{F'P'}^2 - \left(r_{F'P'} - \dfrac{\sigma_{F'}}{\sigma_{P'}}\right)^2 - \left(\dfrac{\langle P'\rangle - \langle F'\rangle}{\sigma_{P'}}\right)^2 + \left(\dfrac{\langle P'\rangle}{\sigma_{P'}}\right)^2}{1 + \left(\dfrac{\langle P'\rangle}{\sigma_{P'}}\right)^2} \quad \textbf{(4)}$$

221   where *F* is the "forecast" (i.e. the 12 km simulations mapped to 60 km, WRF12-remap); *P* is

Atmospheric
Chemistry
and Physics
Discussions

222   the "target" (i.e. MODIS at 60 km) and output from WRF60 are used as the reference forecast;

223   *F'* the difference between 12 km estimates regridded to 60 km and MODIS; *P'* the difference

224   between the 60 km simulation and MODIS.

225   BSS measure the improvement in the accuracy with which WRF12-remap reproduces

226   observations (from MODIS, MERRA-2 or other satellite products) over output from WRF60.

227   A BSS>0 indicates WRF12, even when regridded to 60 km, does add value. The first term in

228   (4) ranges from 0 to 1, is described as the potential skill, and is the square of the spatial

229   correlation coefficient between forecast and reference anomalies to MODIS. It is the skill score

230   achievable if both the conditional and overall bias were zero, and for most of the variables

231   considered herein (particularly AOD) it contributes to a positive BSS in most calendar months

232   (and seasons). The second term (the conditional bias, > 0), is the square of the difference

233   between the anomaly correlation coefficient and the ratio of standard deviation of the

234   anomalies. The third term is referred to as the forecast anomaly bias, and is the ratio of the

235   difference between the mean anomalies of WRF12-remap and the observations relative to

236   WRF60 and the standard deviation of WRF60 anomaly relative to observed values. The fourth

237   term is the degree of agreement and appears in both the numerator and denominator. It is

238   computed as the square of the ratio of the mean anomaly between WRF60 and observations

239   and the standard deviation of the anomalies.

240   **(ii) Pooled paired t-test**

241   To identify which areas in space contribute most to the added value, we compare daily mean

242   AOD fields from WRF-Chem at different resolutions and MODIS. We perform a pooled paired

243   t-test to evaluate the null hypothesis that those differences come from normal distributions with

244   equal means and equal but unknown variances (the test statistic has Student's *t* distribution with

245   df = n + m − 2, and the sample standard deviation is the pooled standard deviation, where n

246   and m are the two sample sizes). The test is conducted by climatological season (e.g. winter =

247   DJF) since there are fewer than 20 valid AOD observations in most 60 km grid cells for each

248   calendar month (Fig. 2). Given the large number of hypothesis tests performed (i.e. one for

249   each 60 km grid cell), we adjust the p-values using the False Discovery Rate (FDR) approach

250   (Benjamini and Hochberg, 1995). In this approach, p-values from the t-tests are ranked from

251   low to high ($p_1, p_2, \ldots, p_m$), then the test with the highest rank, *j*, satisfying:

252    $$p_j \leq \frac{j}{m} \alpha \quad \textbf{(5)}$$

Atmospheric
Chemistry
and Physics
Discussions

253   is identified. Here all p-values satisfying Eq. 5 with α=0.1 are considered significant.

254   **(iii) Accuracy and Hit Rate in identification of extremes**

255   For each month we identify grid cells in which the wavelength specific AOD exceeds the 75th

256   percentile value computed from all grid cells and define that as an extreme. Thus grid cells

257   with extreme AOD are independently determined for MODIS and WRF-Chem at different

258   resolutions. The spatial coherence in identification of extremes in the fields is quantified using

259   two metrics: the *Accuracy* and the *Hit Rate* (*HR*). The *Accuracy* indicates the overall spatial

260   coherence and is computed as the number of grid cells co-identified as extreme and non-

261   extreme between WRF-Chem and MODIS relative to the total number of cells with valid data.

262   The *HR* weights only correct identification of extremes in MODIS by WRF-Chem.

263   **3 Results**

264   **3.1 Quantifying the value added of increased spatial resolution**

265   When WRF-Chem is applied at 60 km resolution the degree of association of the resulting

266   spatial fields of mean monthly AOD at the three wavelengths with MODIS varies seasonally.

267   Smallest RMSD and highest Spearman spatial correlations (ρ) with MODIS observations

268   generally occur during months with highest mean AOD (i.e. during summer, Fig. 1 and 3), and

269   reach a maximum in August (ρ = 0.60, Table 1). However, while the patterns of relative AOD

270   variability are well captured, the absolute magnitudes and spatial gradients of AOD during the

271   summer are underestimated by WRF60 (Fig. 1 and Fig. 3, Table S2). High spatial correlations

272   (ρ > 0.40) are also observed in March, April and November (Table 1), when the ratio of spatial

273   standard deviations is closer to 1 (Fig. 1, Table S2). Only a weak wavelength dependence is

274   observed in the performance metrics as described on Taylor diagrams. The spatial variability

275   is generally more negatively biased for AOD at 660 nm (Table S2), indicating that WRF60

276   simulations tend to produce larger diameter aerosols homogeneously distributed over the

277   domain, whereas MODIS observations indicate more spatial variability.

278   The performance of WRF60 simulations relative to MODIS contrasts with analyses of WRF12

279   and WRF12-remap. WRF12 and WRF12-remap indicate highest spatial correlations with

280   MODIS observations throughout the summer months (ρ = 0.5-0.7, Table 1), although the bias

281   towards simulation of more coarse aerosols than are observed is consistent across the two

282   simulations and with prior research (see details provided in (Crippa et al., 2016)). However,

283   simulations at 12 km (WRF12) show positive ρ with MODIS for all λ in all calendar months,

284   while mean monthly spatial fields of AOD from WRF60 show low and/or negative correlations

Atmospheric
Chemistry
and Physics
Discussions

285   with MODIS during May, June, September, October and December, indicating substantial

286   differences in the degree of correspondence with MODIS AOD in the two simulations, and

287   higher fidelity of the enhanced resolution runs (Tables 1 and S2).

288   Monthly mean spatial fields of AOD(λ) as simulated by WRF12 or WRF12-remap exhibit

289   positive Spearman correlation coefficients (ρ) with MODIS observations for all calendar

290   months and range from ~ 0.25 for WRF12-remap (0.20 for WRF12) during winter to ~ 0.70

291   and 0.64, respectively during summer (Table 1). Spearman's ρ are uniformly higher in WRF12-

292   remap than WRF12 indicating a mismatch in space in the high-resolution simulation (i.e. that

293   grid cells with high AOD are slightly displaced in the 12 km simulations possibly due to the

294   presence of sub-grid scale aerosol plumes (Rissman et al., 2013)). Mean monthly fields of AOD

295   (all λ) from both WRF12 and WRF12-remap exhibit lower ρ with MODIS in February-April

296   and November than the 60 km runs (Table 1). These discrepancies appear to be driven by

297   conditions in the south of the domain. For example, differences between WRF60/WRF12-

298   remap vs. MODIS during all seasons are significant according to the paired t-test over Florida

299   and along most of the southern coastlines (Fig. 2). This region of significant differences extends

300   up to ~ 40°N during summer and fall, reflecting the stronger north-south gradient in AOD from

301   MODIS and WRF12-remap that is not captured by WRF60 (see example for λ = 550 nm, Fig.

302   3). These enhancements in the latitudinal gradients from WRF12-remap are also manifest in

303   the physical variables (particularly specific humidity as discussed further below).

304   The differences in the absolute values of mean monthly AOD deriving from differences in the

305   resolution at which WRF-Chem was applied are of sufficient magnitude (a difference of up to

306   0.2 in regions with a mean AOD value of 0.4), particularly in the summer months (Fig. 4), to

307   raise concerns. However, detailed investigation of the simulations settings and repetition of the

308   60 km simulation resulted in virtually identical results indicating no fault can be found in the

309   analysis. Further, we note this is a region of high discrepancy in global ESM (Myhre et al.,

310   2013a).

311   To further investigate differences due to spatial discretization we computed Brier Skill Scores

312   (BSS, Eq. 4). In this analysis AOD for each λ from WRF12-remap are used as the 'forecast',

313   output from WRF60 are used as the reference forecast and MODIS observations at 60 km are

314   used as the target. BSS exceed 0 during all months except for September and October, and

315   largest BSS (> 0.5) for AOD (all λ) is found during most months between December and July

316   (Fig. 5). This indicates that running WRF-Chem at 12 km resolution adds value relative to

317 WRF60, even when the WRF12 output is remapped to 60 km. BSS do not strongly depend on

318 λ, indicating the added value from enhanced resolution similarly affects particles of different

319 sizes. Inspecting the terms defining the BSS provides information about the origin of the added

320 value (Fig. 5). The positive BSS derives principally from the potential skill (first term in Eq.

321 4), which demonstrates a reduction in bias and/or more accurate representation of the spatial

322 gradients in WRF12-remap. This term exhibits a weak seasonality with values below 0.5 only

323 during August and fall months. The second and third terms are close to zero during most

324 months, although bigger biases are found during August-October. The substantial conditional

325 bias during late summer and early fall is the result of the large ratio of standard deviations (>

326 1, i.e. the spatial variability of the anomaly relative to MODIS is larger for WRF12-remap than

327 WRF60, Table S2). It thus contributes to the negative BSS found in September and October,

328 which are also identified as outlier months in WRF12-remap from the Taylor diagram analysis

329 (Fig. 1). Output for these months show modest spatial correlations with MODIS and higher

330 ratio of standard deviations than in WRF60-MODIS comparisons (Fig. 1, Table S2).

331 Model resolution also affects the *Accuracy* and *Hit Rate* (*HR*) for identification of areas of

332 extreme AOD (AOD>75th percentile). Highest coherence in the identification of extreme AOD

333 in space identified in WRF12-remap (and WRF12) relative to MODIS is found during May-

334 August (*HR* = 53-77%) vs. WRF60 (*HR* = 17-54%, Table 2). Conversely highest *HR* are found

335 for WRF60 and MODIS during winter and early spring, and indeed exceed those for WRF12

336 and WRF12-remap (Table 2, e.g. Feb: *HR* = 0.78 for WRF60, and 0.67 and 0.68 for WRF12

337 and WRF12-remap, respectively). These differences are consistent with the observation that

338 WRF12-remap overestimates the scales of AOD coherence and AOD magnitude during the

339 cold season along coastlines and over much of the domain in April (Fig. 3).

340 The synthesis of these analyses is thus that the higher resolution simulation increases the

341 overall spatial correlation, decreases overall bias in AOD close to the peak of the solar spectrum

342 relative to MODIS observations and therefore the higher-resolution simulations better

343 represent aerosol direct climate forcing. However, WRF12-remap exhibits little improvement

344 over WRF60 in terms of reproducing the spatial variability of AOD at these wavelengths and

345 further that WRF12-remap tends to be more strongly positively biased in terms of mean

346 monthly AOD outside of the summer months (Fig. 2 and Fig. 3). Also the improvement in

347 detection of areas of extreme AOD in the higher resolution simulations (WRF12-remap) is

348 manifest only during the warm season.

3.2 Investigating the origin of the added value and sources of error in simulated AOD

As documented above, WRF-Chem applied at either 60 or 12 km resolution over eastern North America exhibits some skill in reproducing observed spatial fields of AOD and the occurrence of extreme AOD values. However, marked discrepancies both in space and time are found, and at least some of them show a significant dependence on model resolution. Thus, we investigated a range of physical conditions and gas phase concentrations known to be strongly determinant of aerosol dynamics in terms of the BSS as a function of model resolution and also in terms of the mean monthly spatial patterns.

WRF12 even when remapped to 60 km provides more accurate description of key meteorological variables such as specific humidity (Q), *PBLH*, surface temperature and precipitation (Fig. 6, S1, S2 and S3) when comparing to MERRA-2, as indicated by the positive BSS during almost all months (Fig. 7a). Good qualitative agreement is observed for the spatial patterns and absolute magnitude of T_{2m} in both WRF60 and WRF12-remap relative to MERRA-2 for all seasons (Fig. S1) leading to only modest magnitude of BSS (i.e. value added by the higher resolution simulations (Fig. 7a). The aerosol size distribution and therefore wavelength specific AOD exhibits a strong sensitivity to Q (Santarpia et al., 2005) due to the presence of hygroscopic components in atmospheric aerosols and thus the role of water uptake in determining aerosol diameter, refractivity and extinction coefficient (Zieger et al., 2013). For example, the hygroscopic growth factor, which indicates the change of aerosol diameter due to water uptake, is ~ 1.4 for pure ammonium sulfate with dry diameter of 532 nm at relative humidity of 80%, thus biases in representation atmospheric humidity may lead to big errors in simulated aerosol size and AOD (Flores et al., 2012). Our previous analyses of the 12 km resolution simulations indicated overestimation of sulfate aerosols (a highly hygroscopic aerosol component, and one which in many chemical forms exhibits strong hysteresis (Martin et al. 2004)) relative to observed near-surface $PM_{2.5}$ concentrations during all seasons except for winter (Crippa et al., 2016), leading to the hypothesis that simulated AOD and discrepancies therein may exhibit a strong dependence on Q. Consistent with that postulate, Q_{PBL} from WRF12-remap exhibits a wet bias in cloud-free grid cells mostly during warm months, whereas WRF60 is characterized by a dry bias during all seasons (Fig. 6). Despite the positive bias, WRF12-remap better captures the seasonal spatial patterns of Q_{PBL} in MERRA-2, leading to positive BSS in all calendar months. Thus, there is added value by higher-resolution simulations in representation of one of the key parameters dictating particle growth and optical properties. Spatial patterns of differences in Q_{PBL} from WRF60 and WRF12-remap relative to

Atmospheric
Chemistry
and Physics
Discussions

Open Access

EGU

382   MERRA-2 (Fig. 6) exhibit similarities to differences in AOD (Fig. 4). WRF60 is dry-biased

383   relative to WRF12 particularly during the summer (and fall) and underestimates Q_{PBL} relative

384   to MERRA-2 during all seasons over the southern states and over most of continental US

385   during summer and fall. Conversely, WRF12-remap overestimates Q_{PBL} over most of

386   continental US during summer and fall relative to MERRA-2.

387   *PBLH* is a key variable for dictating near-surface aerosol concentrations but is highly sensitive

388   to the physical schemes applied, and biases appear to be domain and resolution dependent. For

389   example, the Mellor-Yamada-Janjich *PBL* scheme combined with the Noah Land Surface

390   Model applied in this work was found to produce lower *PBL* heights (Zhang et al., 2009) than

391   other parameterizations. Thus, the positive bias in simulated AOD and surface $PM_{2.5}$

392   concentrations (reported previously in (Crippa et al., 2016)) may be linked to the systematic

393   underestimation of *PBLH* simulated by WRF12-remap over continental US relative to

394   MERRA-2 during all seasons (except winter) with greatest bias over regions of complex

395   topography (Fig. S2). However, a positive bias (of several hundred meters) in terms of *PBLH*

396   for WRF simulations using the MYJ parameterization was previously reported for high-

397   resolution simulations over complex terrain (Rissman et al., 2013), and a positive bias in *PBLH*

398   is also observed in the 60 km simulations presented herein (Fig. S2). This may provide a partly

399   explanation for the strong negative bias in AOD in WRF60 during summer (Fig. 3). In general,

400   the BSS indicate improvement in the simulation of *PBLH* in WRF12-remap than in WRF60

401   (Fig. 7a). Consistent with the dry bias in Q_{PBL} in WRF60, total accumulated precipitation is

402   also underestimated in WRF60, while WRF12-remap captures the absolute magnitudes and the

403   spatial patterns therein (Fig. S3). Analysis of hourly precipitation rates also showed higher skill

404   of WRF12-remap than WRF60 in correctly simulating precipitation occurrence (*HR*) relative

405   to MERRA-2 (Table S3). More specifically WRF12-remap correctly predicts between 40%

406   and 70 % of precipitation events in MERRA-2 with highest skill during winter months, whereas

407   WRF60 output exhibits lower HR (~6% during summer and 30% during winter). This result

408   thus confirms our expectation of a strong sensitivity of model performance to resolution due to

409   the inherent scale dependence in the cumulus scheme.

410   Gas phase concentrations (transformed into z-scores) from WRF12-remap show higher

411   agreement with satellite observations during almost all months, as indicated by the positive

412   BSS (Fig. 7b). However given the limited availability of valid satellite observations (especially

413   during months with low radiation intensity), the BSS are likely only robust for the summer

414   months for all species. Nevertheless, with the exception of NH_3 during June, BSS for all months

Atmospheric
Chemistry
and Physics
Discussions

415   are above or close to zero indicating on average, the enhanced resolution simulations do

416   improve the quality of the simulation of the gas phase species even when remapped to 60 km

417   resolution. Further, the seasonal average spatial patterns of the total columnar concentrations,

418   expressed in terms of z-scores, also exhibit high qualitative agreement with the satellite

419   observations (Fig. S4-S7).

420   **4 Concluding remarks**

421   This analysis is one of the first to quantify the impact of model spatial resolution on the spatio-

422   temporal variability and magnitude of AOD. Application of WRF-Chem at two different

423   resolutions (60 km and 12 km) over eastern North America for a representative year (2008)

424   leads to the following conclusions:

425   -   Higher resolution simulations add value (i.e. enhance the fidelity of AOD at and near

426   to the peak in the solar spectrum) relative to a coarser run, although the improvement

427   in model performance is not uniform in space and time. Brier Skill Scores for the

428   remapped simulations (i.e. output from simulations conducted at 12 km (WRF12) then

429   averaged to 60 km, WRF12-remap) are positive for ten of twelve calendar moths, and

430   for AOD(λ=550 nm) exceed 0.5 for seven of twelve months.

431   -   Spatial correlations of output from WRF12 and WRF12-remap with observations from

432   MODIS are higher than output from a simulation conducted at 60 km during most

433   months. For example, in contrast to WRF-Chem simulations at 60 km (WRF60),

434   simulations conducted at 12 km (WRF12) show positive spatial correlations with

435   MODIS for all λ in all calendar months, and particularly during summer (ρ = 0.5-0.7).

436   -   Output from WRF12 and WRF12-remap exhibit highest accord with MODIS

437   observations in capturing the frequency, magnitude and location of extreme AOD

438   values during summer when AOD is typically highest. During May-August WRF12-

439   remap has Hit Rates for identification of extreme AOD of 53-78%.

440   -   At least some of the improvement in the accuracy with which AOD is reproduced in

441   the higher resolution simulations may be due to improved fidelity of specific humidity

442   and thus more accurate representation of hygroscopic growth of some aerosol

443   components.

444   -   Higher-resolution simulations add value in the representation of key meteorological

445   variables such as temperature, boundary layer height and precipitation. Both spatial

446   patterns and precipitation occurrence are better captured by WRF12-remap.

15

447   -   More accurate representation of spatial patterns and magnitude of gaseous species

448   playing a key role in particle formation and growth is achieved by running WRF-Chem

449   at high resolution.

450   It is worthy of note that even the 12 km resolution WRF-Chem simulations exhibit substantial

451   differences in AOD relative to MODIS over eastern North America, and the agreement varies

452   only slightly with wavelength. This may be partially attributable to use of the modal approach

453   to represent the aerosol size distribution in order to enhance computational tractability. In this

454   application each mode has a fixed geometric standard deviation (σ_g), which can lead to biases

455   in simulated AOD in the visible wavelengths by up to 25% (Brock et al., 2016) (with the model

456   overestimating observations if the prescribed σ_g is larger than the observed one). Setting $\sigma_g =$

457   2 for the accumulation mode (the default in WRF-Chem) may lead to an overestimation of the

458   number of particles at the end of the accumulation mode tail, and there is evidence that a value

459   of $\sigma_{g,acc}$=1.40 leads to higher agreement with observations (Mann et al., 2012). Further possible

460   sources of the AOD biases reported herein derive from selection of the physical schemes (e.g.

461   planetary boundary layer (*PBL*) schemes and land-surface model (Misenis and Zhang,

462   2010;Zhang et al., 2009)). Further, it is worth mentioning that NEI emissions are specified

463   based on an average summertime weekday, so higher model performance might be achieved if

464   seasonally varying emissions would be available. Future work will include a systematic

465   sensitivity analysis of these effects.

Acknowledgments

Atmospheric
Chemistry
and Physics
Discussions

Open Access

References

477 **References**

478 Ackermann, I. J., Hass, H., Memmesheimer, M., Ebel, A., Binkowski, F. S., and Shankar, U.:
479 Modal aerosol dynamics model for Europe: development and first applications, Atmos.
480 Environ., 32, 2981-2999, http://dx.doi.org/10.1016/S1352-2310(98)00006-5, 1998.

481 Anderson, T. L., Charlson, R. J., Winker, D. M., Ogren, J. A., and Holmén, K.: Mesoscale
482 Variations of Tropospheric Aerosols, Journal of the Atmospheric Sciences, 60, 119-136, doi:
483 http://dx.doi.org/10.1175/1520-0469(2003)060<0119:MVOTA>2.0.CO;2, 2003.

484 Ångström, A.: The parameters of atmospheric turbidity, Tellus, 16, 64-75, 10.1111/j.2153-
485 3490.1964.tb00144.x, 1964.

486 Benjamini, Y., and Hochberg, Y.: Controlling the False Discovery Rate: A Practical and
487 Powerful Approach to Multiple Testing, Journal of the Royal Statistical Society. Series B
488 (Methodological), 57, 289-300, 1995.

489 Boucher, O., D. Randall, P. Artaxo, C. Bretherton, G. Feingold, P. Forster, V.-M. Kerminen,
490 Y. Kondo, H. Liao, U. Lohmann, P. Rasch, S.K. Satheesh, S. Sherwood, B. Stevens and X.Y.
491 Zhang: Clouds and Aerosols, in: Climate Change 2013: The Physical Science Basis.
492 Contribution of Working Group I to the Fifth Assessment Report of the Intergovernmental
493 Panel on Climate Change, edited by: Stocker, T. F., D. Qin, G.-K. Plattner, M. Tignor, S.K.
494 Allen, J. Boschung, A. Nauels, Y. Xia, V. Bex and P.M. Midgley, Cambridge University Press,
495 Cambridge, United Kingdom and New York, NY, USA, 33–115, 2013.

496 Brinksma, E. J., K. F. Boersma, P. F. Levelt, and R. D. McPeters OMI validation requirements
497 document, Version 1, Rep. RS-OMIE-KNMI-345, 66, 2003.

498 Brock, C. A., Wagner, N. L., Anderson, B. E., Attwood, A. R., Beyersdorf, A., Campuzano-
499 Jost, P., Carlton, A. G., Day, D. A., Diskin, G. S., Gordon, T. D., Jimenez, J. L., Lack, D. A.,
500 Liao, J., Markovic, M. Z., Middlebrook, A. M., Ng, N. L., Perring, A. E., Richardson, M. S.,
501 Schwarz, J. P., Washenfelder, R. A., Welti, A., Xu, L., Ziemba, L. D., and Murphy, D. M.:
502 Aerosol optical properties in the southeastern United States in summer – Part 1: Hygroscopic
503 growth, Atmos. Chem. Phys., 16, 25695-25738, doi:10.5194/acp-16-5009-2016, 2016.

504 Chance, K.: OMI algorithm theoretical basis document, volume IV: OMI trace gas algorithms,
505 2002.

506 Chin, M., Kahn, R. A., and Schwartz , S. E.: Atmospheric Aerosols Properties and Climate
507 Impacts. A Report by the U.S. Climate Change Science Program and the Subcommittee on
508 Global Change Research, in, National Aeronautics and Space Administration, Washington,
509 D.C., USA, 128, 2009.

510 Crippa, P., Sullivan, R. C., Thota, A., and Pryor, S. C.: Evaluating the skill of high-resolution
511 WRF-Chem simulations in describing drivers of aerosol direct climate forcing on the regional
512 scale, Atmos. Chem. Phys., 16, 397-416, 10.5194/acp-16-397-2016, 2016.

513 Di Luca, A., de Elía, R., and Laprise, R.: Challenges in the Quest for Added Value of Regional
514 Climate Dynamical Downscaling, Curr Clim Change Rep, 1, 10-21, 10.1007/s40641-015-
515 0003-9, 2015.

516   Diaconescu, E., and Laprise, R.: Can added value be expected in RCM-simulated large scales?,
517   Clim Dyn, 41, 1769-1800, 10.1007/s00382-012-1649-9, 2013.

518   Emmons, L. K., Walters, S., Hess, P. G., Lamarque, J. F., Pfister, G. G., Fillmore, D., Granier,
519   C., Guenther, A., Kinnison, D., Laepple, T., Orlando, J., Tie, X., Tyndall, G., Wiedinmyer, C.,
520   Baughcum, S. L., and Kloster, S.: Description and evaluation of the Model for Ozone and
521   Related chemical Tracers, version 4 (MOZART-4), Geoscientific Model Development, 3, 43-
522   67, doi:10.5194/gmd-3-43-2010, 2010.

523   Fioletov, V. E., McLinden, C. A., Krotkov, N., Moran, M. D., and Yang, K.: Estimation of SO_2
524   emissions using OMI retrievals, Geophysical Research Letters, 38, L21811,
525   10.1029/2011GL049402, 2011.

526   Flores, J. M., Bar-Or, R. Z., Bluvshtein, N., Abo-Riziq, A., Kostinski, A., Borrmann, S., Koren,
527   I., Koren, I., and Rudich, Y.: Absorbing aerosols at high relative humidity: linking hygroscopic
528   growth to optical properties, Atmospheric Chemistry and Physics, 12, 5511-5521,
529   10.5194/acp-12-5511-2012, 2012.

530   Grell, G. A., Peckham, S. E., Schmitz, R., McKeen, S. A., Frost, G., Skamarock, W. C., and
531   Eder, B.: Fully coupled "online" chemistry within the WRF model, Atmos. Environ., 39, 6957-
532   6975, 10.1016/j.atmosenv.2005.04.027, 2005.

533   Hyer, E. J., Reid, J. S., and Zhang, J.: An over-land aerosol optical depth data set for data
534   assimilation by filtering, correction, and aggregation of MODIS Collection 5 optical depth
535   retrievals, Atmospheric Measurement Techniques, 4, 379-408, 10.5194/amt-4-379-2011,
536   2011.

537   Krotkov, N. A., McClure, B., Dickerson, R. R., Carn, S. A., Li, C., Bhartia, P. K., Yang, K.,
538   Krueger, A. J., Li, Z., Levelt, P. F., Chen, H., Wang, P., and Lu, D.: Validation of SO_2 retrievals
539   from the Ozone Monitoring Instrument over NE China, Journal of Geophysical Research:
540   Atmospheres, 113, D16S40, 10.1029/2007JD008818, 2008.

541   Leibensperger, E., Mickley, L. J., Jacob, D. J., Chen, W.-T., Seinfeld, J., Nenes, A., Adams,
542   P., Streets, D., Kumar, N., and Rind, D.: Climatic effects of 1950–2050 changes in US
543   anthropogenic aerosols–Part 1: Aerosol trends and radiative forcing, Atmospheric Chemistry
544   and Physics, 12, 3333-3348, doi:10.5194/acp-12-3333-2012, 2012.

545   Levy, R. C., Mattoo, S., Munchak, L. A., Remer, L. A., Sayer, A. M., Patadia, F., and Hsu, N.
546   C.: The Collection 6 MODIS aerosol products over land and ocean, Atmospheric Measurement
547   Techniques, 6, 2989-3034, 10.5194/amt-6-2989-2013, 2013.

548   Long, M., Yantosca, R., Nielsen, J., Keller, C., da Silva, A., Sulprizio, M., Pawson, S., and
549   Jacob, D.: Development of a grid-independent GEOS-Chem chemical transport model (v9-02)
550   as an atmospheric chemistry module for Earth system models, Geoscientific Model
551   Development, 8, 595-602, doi:10.5194/gmd-8-595-2015, 2015.

552   Mann, G. W., Carslaw, K. S., Ridley, D. A., Spracklen, D. V., Pringle, K. J., Merikanto, J.,
553   Korhonen, H., Schwarz, J. P., Lee, L. A., Manktelow, P. T., Woodhouse, M. T., Schmidt, A.,
554   Breider, T. J., Emmerson, K. M., Reddington, C. L., Chipperfield, M. P., and Pickering, S. J.:
555   Intercomparison of modal and sectional aerosol microphysics representations within the same

Atmospheric
Chemistry
and Physics
Discussions

556   3-D global chemical transport model, Atmospheric Chemistry and Physics, 12, 4449-4476,
557   10.5194/acp-12-4449-2012, 2012.

558   Martin, S. T., Hung, H. M., Park, R. J., Jacob, D. J., Spurr, R. J. D., Chance, K. V., and Chin,
559   M.: Effects of the physical state of tropospheric ammonium-sulfate-nitrate particles on global
560   aerosol direct radiative forcing, Atmospheric Chemistry and Physics, 4, 183-214,
561   doi:10.5194/acp-4-183-2004, 2004.

562   McComiskey, A., Schwartz, S. E., Schmid, B., Guan, H., Lewis, E. R., Ricchiazzi, P., and
563   Ogren, J. A.: Direct aerosol forcing: Calculation from observables and sensitivities to inputs,
564   Journal of Geophysical Research: Atmospheres, 113, D09202, 10.1029/2007JD009170, 2008.

565   McLinden, C. A., Fioletov, V., Boersma, K. F., Kharol, S. K., Krotkov, N., Lamsal, L., Makar,
566   P. A., Martin, R. V., Veefkind, J. P., and Yang, K.: Improved satellite retrievals of NO_2 and
567   SO_2 over the Canadian oil sands and comparisons with surface measurements, Atmos. Chem.
568   Phys., 14, 3637-3656, 10.5194/acp-14-3637-2014, 2014.

569   Meehl, G. A., Moss, R., Taylor, K. A., Eyring, V., Stouffer, R. J., Sandrine, B., and Stevens,
570   B.: Climate model intercomparisons: preparing for the next phase, Eos, Transaction, American
571   Geophysical Union, 95, 77-84, doi:10.1002/2014EO09, 2014.

572   Misenis, C., and Zhang, Y.: An examination of sensitivity of WRF/Chem predictions to
573   physical parameterizations, horizontal grid spacing, and nesting options, Atmospheric
574   Research, 97, 315-334, 10.1016/j.atmosres.2010.04.005, 2010.

575   Molod, A., Takacs, L., Suarez, M., and Bacmeister, J.: Development of the GEOS-5
576   atmospheric general circulation model: evolution from MERRA to MERRA2, Geoscientific
577   Model Development, 8, 1339-1356, 10.5194/gmd-8-1339-2015, 2015.

578   Murphy, A. H., and Epstein, E. S.: Skill scores and correlation-coefficients in model
579   verification, Monthly Weather Review, 117, 572-581, 10.1175/1520-
580   0493(1989)117<0572:ssacci>2.0.co;2, 1989.

581   Myhre, G., Samset, B. H., Schulz, M., Balkanski, Y., Bauer, S., Berntsen, T. K., Bian, H.,
582   Bellouin, N., Chin, M., Diehl, T., Easter, R. C., Feichter, J., Ghan, S. J., Hauglustaine, D.,
583   Iversen, T., Kinne, S., Kirkevag, A., Lamarque, J. F., Lin, G., Liu, X., Lund, M. T., Luo, G.,
584   Ma, X., van Noije, T., Penner, J. E., Rasch, P. J., Ruiz, A., Seland, O., Skeie, R. B., Stier, P.,
585   Takemura, T., Tsigaridis, K., Wang, P., Wang, Z., Xu, L., Yu, H., Yu, F., Yoon, J. H., Zhang,
586   K., Zhang, H., and Zhou, C.: Radiative forcing of the direct aerosol effect from AeroCom Phase
587   II simulations, Atmospheric Chemistry and Physics, 13, 1853-1877, 10.5194/acp-13-1853-
588   2013, 2013a.

589   Myhre, G., Shindell, D., Bréon, F.-M., Collins, W., Fuglestvedt, J., Huang, J., Koch, D.,
590   Lamarque, J.-F., Lee, D., Mendoza, B., Nakajima, T., Robock, A., Stephens, G., Takemura, T.,
591   and Zhang, H.: Anthropogenic and Natural Radiative Forcing, in: Climate Change 2013: The
592   Physical Science Basis. Contribution of Working Group I to the Fifth Assessment Report of
593   the Intergovernmental Panel on Climate Change, edited by: Stocker, T. F., Qin, D., Plattner,
594   G.-K., Tignor, M., Allen, S. K., Boschung, J., Nauels, A., Xia, Y., Bex, V., and Midgley, P.
595   M., Cambridge University Press, Cambridge, United Kingdom and New York, NY, USA, 659–
596   740, 2013b.

Atmospheric
Chemistry
and Physics
Discussions

597 Rissman, J., Arunachalam, S., Woody, M., West, J. J., BenDor, T., and Binkowski, F. S.: A
598 plume-in-grid approach to characterize air quality impacts of aircraft emissions at the
599 Hartsfield–Jackson Atlanta International Airport, Atmos. Chem. Phys., 13, 9285-9302,
600 10.5194/acp-13-9285-2013, 2013.

601 Rockel, B., Castro, C. L., Pielke, R. A., von Storch, H., and Leoncini, G.: Dynamical
602 downscaling: Assessment of model system dependent retained and added variability for two
603 different regional climate models, Journal of Geophysical Research: Atmospheres, 113,
604 D21107, 10.1029/2007JD009461, 2008.

605 Santarpia, J. L., Gasparini, R., Li, R. J., and Collins, D. R.: Diurnal variations in the
606 hygroscopic growth cycles of ambient aerosol populations, J. Geophys. Res.-Atmos., 110,
607 10.1029/2004jd005279, 2005.

608 Seinfeld, J. H., and Pandis, S. N.: Atmospheric chemistry and physics: from air pollution to
609 climate change, John Wiley & Sons, 1152 pp., 2016.

610 Simes, R. J.: An improved Bonferroni procedure for multiple tests of significance, Biometrika,
611 73, 751-754, 10.2307/2336545, 1986.

612 Taylor, K. E.: Summarizing multiple aspects of model performance in a single diagram, J.
613 Geophys. Res.-Atmos., 106, 7183-7192, 10.1029/2000jd900719, 2001.

614 Tilmes, S., Lamarque, J.-F., Emmons, L., Kinnison, D., Ma, P.-L., Liu, X., Ghan, S., Bardeen,
615 C., Arnold, S., and Deeter, M.: Description and evaluation of tropospheric chemistry and
616 aerosols in the Community Earth System Model (CESM1. 2), Geoscientific Model
617 Development, 8, 1395-1426, doi:10.5194/gmd-8-1395-2015, 2015.

618 Tomasi, C., Caroli, E., and Vitale, V.: Study of the Relationship between Ångström's
619 Wavelength Exponent and Junge Particle Size Distribution Exponent, Journal of Climate and
620 Applied Meteorology, 22, 1707-1716, 10.1175/1520-
621 0450(1983)022<1707:SOTRBW>2.0.CO;2, 1983.

622 US-EPA: 2005 National Emissions Inventory (NEI), US Environmental Protection Agency in,
623 available at: ftp://aftp.fsl.noaa.gov/divisions/taq/emissions_data_2005/, 2009.

624 Vinken, G. C. M., Boersma, K. F., van Donkelaar, A., and Zhang, L.: Constraints on ship NO_x
625 emissions in Europe using GEOS-Chem and OMI satellite NO_2 observations, Atmos. Chem.
626 Phys., 14, 1353-1369, 10.5194/acp-14-1353-2014, 2014.

627 Whitburn, S., Van Damme, M., Clarisse, L., Bauduin, S., Heald, C., Hadji-Lazaro, J.,
628 Hurtmans, D., Zondlo, M. A., Clerbaux, C., Coheur, P.-F. : A flexible and robust neural
629 network IASI-NH_3 retrieval algorithm, J. Geophys. Res. Atmos, In Press,
630 10.1002/2016JD024828, 2016.

631 Zhang, Y., Dubey, M. K., Olsen, S. C., Zheng, J., and Zhang, R.: Comparisons of WRF/Chem
632 simulations in Mexico City with ground-based RAMA measurements during the 2006-
633 MILAGRO, Atmospheric Chemistry and Physics, 9, 3777-3798, doi:10.5194/acp-9-3777-
634 2009, 2009.

Atmospheric
Chemistry
and Physics
Discussions

Open Access

EGU

635   Zieger, P., Fierz-Schmidhauser, R., Weingartner, E., and Baltensperger, U.: Effects of relative
636   humidity on aerosol light scattering: results from different European sites, Atmospheric
637   Chemistry and Physics, 13, 10609-10631, 10.5194/acp-13-10609-2013, 2013.

638

639

640   **Figures**

641
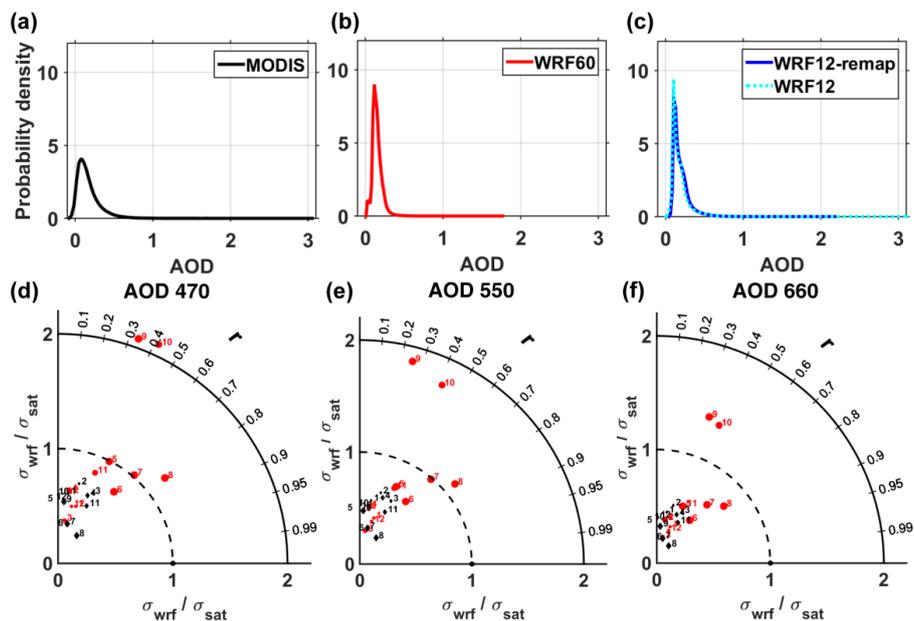
642

643   **Figure 1. Probability density function of once daily AOD at a wavelength (λ) of 550 nm**

644   **for (a) MODIS, (b) WRF60 and (c) WRF12 and WRF12-remap during the year 2008. (d-**

645   **f) Taylor diagrams of mean monthly AOD at wavelengths (λ) of (d) 470, (e) 550 and (f)**

646   **660 nm as simulated by WRF-Chem at different resolutions (black diamonds=WRF60**

647   **and red dots=WRF12-remap) relative to MODIS observations. The numbers by each**

648   **symbol denote the calendar month (e.g. 1=January).**

649
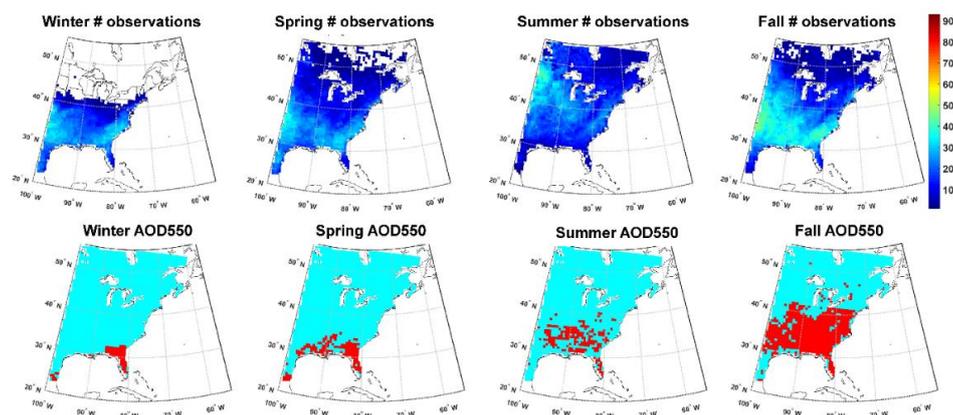
Figure 2. First line: Number of paired AOD observations at a wavelength (λ) of 550 nm (i.e. simultaneous values as output from WRF-Chem and observed by MODIS) used to perform a t-test designed to evaluate whether the difference computed for each grid cell as WRF60-MODIS differs from that computed as WRF12-remap-MODIS on a seasonal basis (columns show Winter (DJF), Spring (MAM), Summer (JJA) and Fall (SON)). Second line: Results of the t-test. Pixels that have p-values that are significantly different at α=0.10 are indicated in red and have been corrected for multiple testing using a False Discovery Rate approach.

Atmospheric
Chemistry
and Physics
Discussions


660
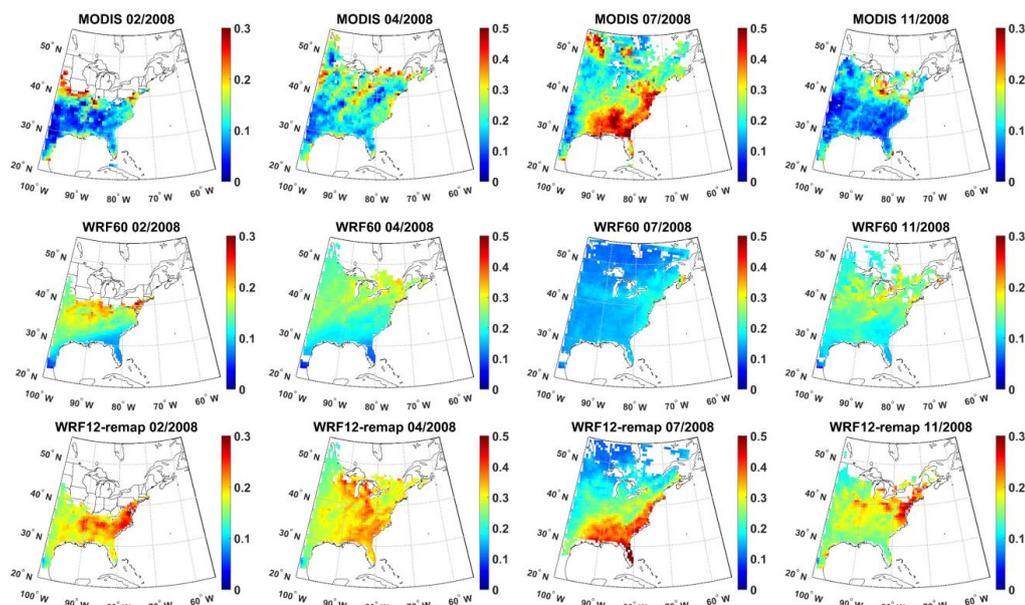
Figure 3. Monthly mean AOD at a wavelength (λ) of 550 nm from MODIS (first line) and

WRF-Chem at different resolutions (WRF60 and WRF12-remap, second and third line)

during a representative month in each climatological season (columns). Note that a

different color scale is applied for different months. For a monthly mean value for a grid

cell to be shown, there must be at least 5-simultaneous daily values (for the time of the

satellite overpass) available.

667

Atmospheric
Chemistry
and Physics
Discussions
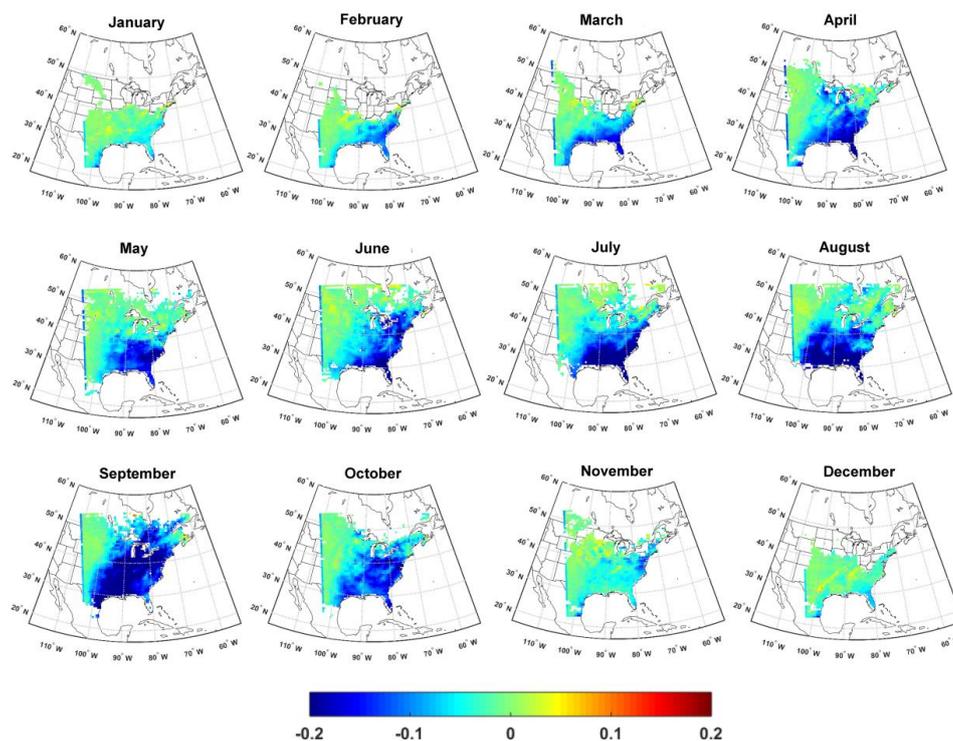
Figure 4. Difference in monthly mean AOD at a wavelength (λ) of 550 nm between WRF-Chem simulations conducted at 60 km resolution (WRF60) and output from WRF-Chem simulations conducted with a resolution of 12 km but remapped to 60 km (WRF12-remap). Differences are computed as WRF60 minus WRF12-remap. Similar spatial patterns and magnitudes of differences are found for λ of 470 and 660 nm. The calendar months of 2008 are shown in the titles of each panel.

676
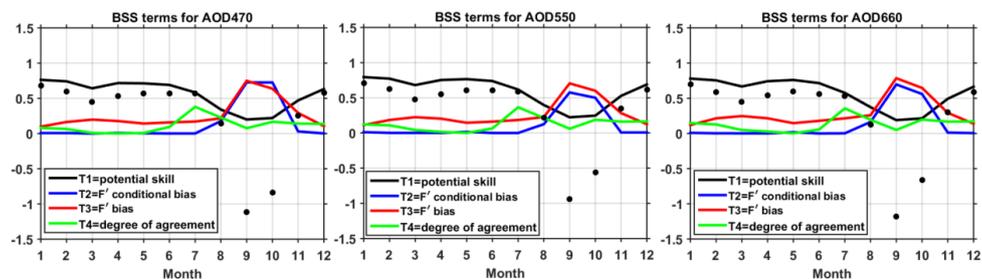
**Figure 5. Brier Skill Scores (BSS, black dots) for monthly mean AOD by calendar month
(1=January) for AOD at 470, 550 and 660 nm. In this analysis of model skill WRF12
output is mapped to the WRF60 grid (WRF12-remap) and BSS are computed using
MODIS as the target, WRF60 as the reference forecast and WRF12-remap as the
forecast. Also shown by the color lines are the contributions of different terms to BSS.**

682

Atmospheric
Chemistry
and Physics
Discussions

683
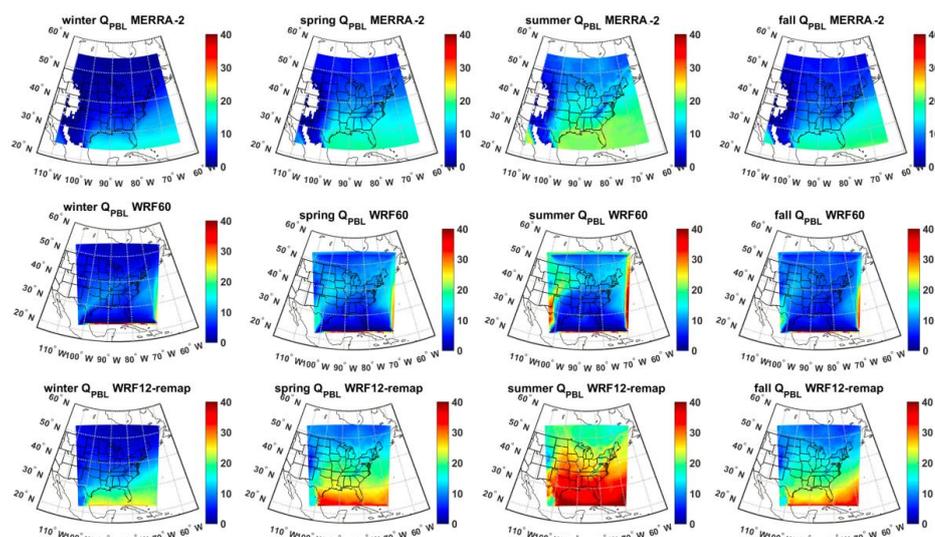
Figure 6. Seasonal mean specific humidity [kg m⁻²] integrated from the surface to 825 hPa

(Q_{PBL}) from MERRA-2 (first row) assuming an average air density in the *PBL* of 1.1 kg

m⁻³, WRF60 (second row), and WRF12-remap (third row). The data are 3-hourly and

show only cloud-free hours in all three data sets.

688

Atmospheric
Chemistry
and Physics
Discussions

Open Access

689
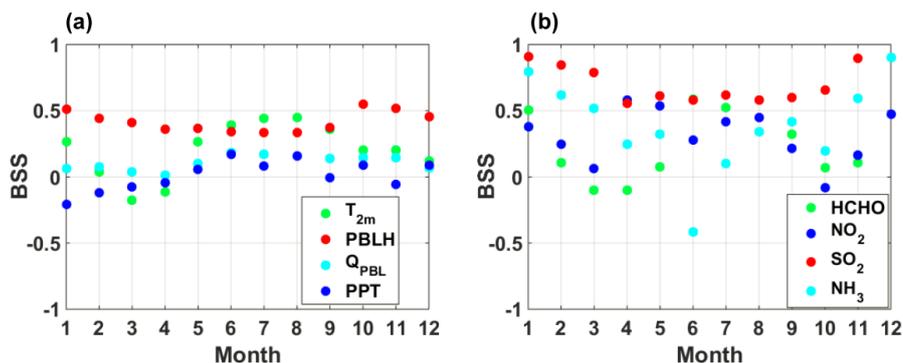
Figure 7. Brier Skill Scores (BSS) for key (a) meteorological and (b) chemical variables.

BSS are computed using hourly data of T at 2m (T_{2m}) and *PBLH*, 3-hourly estimates of

specific humidity in the boundary layer (Q_{PBL}), and z-scores of monthly total precipitation

(*PPT*), and of monthly mean columnar gas phase concentrations.

690

691

692

693

694

695

Atmospheric
Chemistry
and Physics
Discussions

696   **Tables**

697   **Table 1. Spearman correlation coefficients (ρ) between AOD at wavelengths (λ) of 470,**

698   **550 and 660 nm from MODIS observations averaged over 12 or 60 km and WRF-Chem**

699   **simulations conducted at 60 km (WRF60, shown in the table as -60), at 12 km (WRF12,**

700   **shown in the table as -12), and from WRF-Chem simulations at 12 km but remapped to**

701   **60 km (WRF12-remap, shown in the table as -remap). Given WRF12-remap is obtained**

702   **by averaging WRF12 when at least half of the 5×5 12 km resolution cells contain valid**

703   **data, ρ from WRF60 and WRF12-remap may be computed on slightly different**

704   **observations and sample size. The bold text denotes correlation coefficients that are**

705   **significant at α=0.05 after a Bonferroni correction is applied (i.e. $p \leq \dfrac{0.05}{9 \times 12} = 4.63 \times 10^{-4}$**

706   **is significant). The yellow shading is a visual guide that shows for each month and λ the**

707   **model output that has highest ρ with MODIS.**

Month→/Variable↓	Jan	Feb	Mar	Apr	May	Jun	Jul	Aug	Sep	Oct	Nov	Dec
470-12	**0.238**	**0.150**	**0.137**	**0.147**	**0.377**	**0.581**	**0.610**	**0.723**	**0.352**	**0.306**	**0.259**	**0.212**
470-60	0.156	**0.226**	**0.438**	**0.412**	-0.219	-0.146	0.379	**0.601**	0.087	-0.051	**0.500**	-0.059
470-remap	**0.295**	**0.197**	**0.250**	**0.182**	**0.516**	**0.637**	**0.675**	**0.777**	**0.368**	**0.441**	**0.315**	**0.274**
550-12	**0.223**	**0.124**	**0.142**	**0.146**	**0.349**	**0.541**	**0.580**	**0.689**	**0.275**	**0.301**	**0.280**	**0.215**
550-60	**0.179**	**0.244**	**0.429**	**0.332**	-0.288	-0.188	0.324	0.567	0.073	-0.077	**0.491**	0.002
550-remap	**0.297**	0.164	**0.261**	**0.199**	**0.493**	**0.605**	**0.651**	**0.747**	**0.286**	**0.437**	**0.352**	**0.309**
660-12	**0.217**	**0.136**	**0.165**	**0.152**	**0.324**	**0.476**	**0.540**	**0.644**	**0.183**	**0.290**	**0.292**	**0.221**
660-60	**0.191**	**0.230**	**0.437**	**0.402**	-0.305	-0.189	0.389	**0.616**	0.099	-0.137	**0.536**	0.049
660-remap	**0.356**	**0.211**	**0.289**	**0.208**	**0.480**	**0.624**	**0.669**	**0.772**	**0.371**	**0.432**	**0.393**	**0.368**

708

709

Atmospheric
Chemistry
and Physics
Discussions

710 **Table 2. Spatial coherence in the identification of extreme AOD values (i.e. areas with**

711 **AOD>75th percentile over space for each month) between WRF-Chem at different**

712 **resolutions relative to MODIS. No significant wavelength dependence is found for model**

713 **skill in identifying extreme AOD so results are only shown for λ = 550 nm. The different**

714 **model output is denoted by -60 for simulations at 60 km, -12 for simulations at 12 km**

715 **resolution, and as –remap for simulations at 12 km but with the output remapped to 60**

716 **km. The *Accuracy* (Acc) indicates the fraction of grid cells co-identified as extremes and**

717 **non-extremes between WRF-Chem and MODIS relative to the total number of cells with**

718 **valid data. The *Hit Rate* (*HR*) is the probability of correct forecast and is the proportion**

719 **of cells correctly identified as extremes by both WRF-Chem and MODIS. The yellow**

720 **shading indicates the model resolution with highest skill in each month for AOD at 550**

721 **nm.**

Month→/ Metric↓	Jan	Feb	Mar	Apr	May	Jun	Jul	Aug	Sep	Oct	Nov	Dec
Acc-12	0.673	0.665	0.659	0.638	0.710	0.800	0.855	0.839	0.666	0.679	0.723	0.661
Acc-60	0.707	0.778	0.735	0.730	0.600	0.587	0.658	0.769	0.661	0.637	0.729	0.681
Acc-remap	0.674	0.680	0.694	0.640	0.766	0.824	0.887	0.837	0.667	0.699	0.767	0.641
HR-12	0.346	0.331	0.319	0.275	0.421	0.599	0.711	0.678	0.333	0.358	0.447	0.323
HR-60	0.417	0.558	0.471	0.460	0.200	0.173	0.315	0.538	0.321	0.274	0.458	0.364
HR-remap	0.350	0.361	0.387	0.281	0.532	0.649	0.775	0.674	0.333	0.399	0.535	0.284

722

723

724

725

726

727

728

729